research article

Development of a computational pregnant female phantom and calculation of fetal dose during a photon breast radiotherapy

Vjekoslav Kopacin[1,2], Mladen Kasabasic[1,3], Dario Faj[1,4], Marijke de Saint Hubert[5], Stipe Galic[6], Ana Ivkovic[1,3], Marija Majer[7], Hrvoje Brkic[1,4]

[1] Department of Biophysics and Radiology, Faculty of Medicine Osijek, Osijek, Croatia
[2] Department of Diagnostic and Interventional Radiology, Osijek Clinical Hospital Centre, Osijek, Croatia
[3] Department of Medical Physics, Osijek Clinical Hospital Centre, Osijek, Croatia
[4] Department of Biophysics, Biology and Chemistry, Faculty of Dental Medicine and Health in Osijek, Osijek, Croatia
[5] Unit Research in Dosimetric Applications, Belgian Nuclear Research Centre
[6] Department of Medical Physics, University Clinical Hospital Mostar, Mostar, Bosnia and Herzegovina
[7] Division of Materials Chemistry, Ruđer Bošković Institute, Zagreb, Croatia

Vjekoslav Kopacin and Mladen Kasabasic contributed equally.

Radiol Oncol 2022; 56(4): 541-551.

Received 28 July 2022
Accepted DD August 2022

Correspondence to: Assist. Prof. Hrvoje Brkić, Ph.D., Department of Biophysics, Biology and Chemistry, Faculty of Dental Medicine and Health in Osijek, Osijek, Croatia, E-mail: hbrkic@mefos.hr

Disclosure: No potential conflicts of interest were disclosed.

Background. The incidence of carcinoma during pregnancy is reported to be 1:1000–1:1500 pregnancies with the breast carcinoma being the most commonly diagnosed. Since the fetus is most sensitive to ionizing radiation during the first two trimesters, there are mixed clinical opinions and no uniform guidelines on the use of radiotherapy during pregnancy. Within this study the pregnant female phantom in the second trimester, that can be used for radiotherapy treatment planning (as DICOM data), Monte Carlo simulations (as voxelized geometry) and experimental dosimetry utilizing 3D printing of the molds (as .STL files), was developed.

Materials and methods. The developed phantom is based on MRI images of a female patient in her 18th week of pregnancy and CT images after childbirth. Phantom was developed in such a manner that a pregnant female was scanned "*in vivo*" using MRI during pregnancy and CT after childbirth. For the treatment of left breast carcinoma, 3D conformal radiotherapy was used. The voxelized geometry of the phantom was used for Monte Carlo (MC) simulations using Monte Carlo N-Particle transport code™ 6.2 (MCNP).

Conclusions. The modeled photon breast radiotherapy plan, applied to the phantom, indicated that the fetus dose is 59 mGy for 50 Gy prescribed to the breast. The results clearly indicate that only 9.5% of the fetal dose is caused by photons that are generated in the accelerator head through scattering and leakage, but the dominant component is scattered radiation from the patient's body.

Key words: Monte Carlo simulation; phantom; pregnancy; breast neoplasms; radiotherapy; fetal dose

Introduction

The incidence of carcinoma during pregnancy is reported to be 1:1000–1:1500 pregnancies, and according to FIGO 2018 report, the incidence has increased over the last 30 years.[1,2] With an incidence of 1:3000–1:10000, breast carcinoma is the most common malignant tumor during pregnancy.[3-6]

Since the fetus is sensitive to ionizing radiation, mostly during the first two trimesters due

to organogenesis (extendable until the end of the 15th week when the development of the central nervous system ends)[4,7-11], there are mixed clinical opinions and no uniform guidelines on the use of radiotherapy during pregnancy.

According to the National Comprehensive Cancer Network (NCCN) 5.2021 guidelines, radiotherapy is not an option for the treatment of breast carcinoma during pregnancy, yet mastectomy in the first trimester or neoadjuvant chemotherapy and mastectomy in the second trimester.[12] Some authors even suggest abortion in the first trimester, before the treatment has started[8], or in the cases of advanced inoperable cancer stages.[13] Moreover, the Royal College of Obstetricians and Gynecologists Guideline No. 12 considers the use of radiotherapy during pregnancy to be contraindicated.[14] Other authors consider radical mastectomy to be the treatment of choice for the cases in the first trimester or sparing breast surgery during the pregnancy and apply radiotherapy after the childbirth for the cases in the second or third trimester.[1]

According to ICRP 84[9] and ICRP 90 publications[15], as well as in NCRP report 54 and 174[7,16,17], the threshold for the fetus is 50 mGy below which there is no evidence (the risk is considered negligible) for possible congenital malformations, mental retardation, and reduced IQ. Above 50 mGy, and especially for doses above 100 mGy, the risk of stochastic effects increases. Interestingly the ICRP 84 publication states that radiotherapy of malignant diseases outside the pelvis region is possible, which was later also stated in the FIGO 2018 report. Nevertheless, careful planning and accurate dosimetry are strongly advised not to achieve fetal doses above the limit.[2,9,13,18]

Today no consensus exists on how to perform fetal dosimetry which is in practice mostly estimated or measured using computational or modified physical phantoms of pregnant women. For example, a number of groups have performed breast radiotherapy during pregnancy[18-20], but only Antypas *et al*. measured the dose experimentally *in vivo* using TLDs. They have determined that the dose at the fetal position was 36.4 ± 8.6 mGy or 0.079% of the breast dose.[18]

Since the 1960s, dosimetry phantoms have allowed measuring radiation doses in the human body, and since then 121 computer phantoms and 27 physical phantoms of the human body have been developed.[21] Initially, mathematical models[22] were used to calculate the radiation dose, but with advances in computer technology, computational phantoms became a standard in calculating the dose of ionizing radiation in the 1980s. Computer phantoms are categorized into three categories: (1) stylized phantoms, (2) voxelized phantoms, and (3) "boundary representation" (BREP) phantoms.[21] Stylized phantoms were early phantoms, where simple geometric objects that represented the human body were combined. Advances in computer technology, as well as in medical imaging technologies such as computed tomography (CT) and magnetic resonance imaging (MRI), and their wide availability have enabled voxelized phantoms, and BREP phantoms to become the standard for dosimetry studies.

According to the Handbook of Anatomical Models for Radiation Dosimetry[21], among the 121 phantoms, only a few of them are representing pregnant women. First mathematical and stylized models of pregnant females were developed while later RPI-P3, RPI-P6, RPI-P9 Pregnant Women were developed by Oak Ridge National Laboratory (ORNL).[23] Furthermore, KATJA was developed by the National Research Center for Environment and Health in Germany[24] followed by the pregnant female phantom of the Japan Atomic Energy Agency (JAEA) and the UF Family pregnant female library developed by the University of Florida.[25,26] Except for early mathematical and stylized phantoms of ORNL, all the mentioned phantoms were created by separately generating a three-dimensional model of a fetus, obtained from MRI or accidental CT examinations of pregnant women, which were subsequently inserted into an adult women phantom. Due to the huge efforts to build such phantoms and associated costs, these phantoms are often not available to research organizations performing essential research for optimized fetus dosimetry[27] as well as to clinics, requiring such models for fetus dose verification.

All mentioned pregnant phantoms are available only in the digital form, yet their physical representations are still missing. Experimental measurement in dosimetry (using active or passive detectors) can be very complex and they depend on the irradiation set-up, so it is important to have both computational and experimental representations of the phantom. Nevertheless, experimental measurements are required to validate Monte Carlo (MC) simulations, and results from both approaches are complementary. MC simulations can provide information about contributions from different field components, particle types, particle energy spectra, etc. This is useful information when choosing or combining appropriate detectors for experiments and optimization of their calibra-

tions. Our newly developed phantom offers the possibility to obtain the physical representation of the phantom, and calculate the dose on identical geometry, which is novel in dosimetry of pregnant patients.

In this study, a computational anthropomorphic phantom of a woman, in her second trimester of the pregnancy was developed. Woman was imaged during the pregnancy by MRI and after childbirth by CT. Then the feasibility study, to use the phantom for fetal dose calculations using MC simulations, was shown for a photon breast radiotherapy plan. The phantom is made available for treatment planning, in DICOM format as well as a voxelized and mesh format, to be used in Monte Carlo simulations. Finally, the phantom is available in .STL file format, suitable and prepared for 3D printing of the molds, for generation of the physical phantom to be used in further experimental dosimetry.

Materials and methods

Tena phantom creation

Clinical parameters and imaging data

After the faculty's Ethical committee's approval (IRB number: 2158-61-07-21-152, approval date: 14.7.2021.), a pregnant female phantom was developed, named Tena, based on a female patient, of central European descent, in the 18th week of pregnancy, with age 37, body mass of 72 kg (60 kg prior to pregnancy) and body height of 166 cm (BMI 26.1 kg/m^2). The patient signed a written consent authorizing the use of her diagnostic imaging materials to generate this phantom (MR examination of the chest, abdomen, and pelvis obtained during pregnancy and CT examination of the neck, chest, abdomen, and pelvis performed 4 months after delivery). The fetus's gestational age at the moment of performed MRI scan was 17 weeks and 2 days. The estimated fetal mass was calculated as the product of the segmented fetus volume (123.04 cm^3) and the average soft tissue density (1.05 g/cm^3, ICRP 89)[28], and equals 129.2 g. The crown-rump length equals 111.8 mm.

DICOM data from *in vivo* MR scanning of the pregnant female chest, abdomen and pelvis, performed on Siemens Avanto 1,5 T MR scanner as well as DICOM data from performed contrast CT study of the neck, chest, abdomen, and pelvis obtained with Siemens Sensation 40 CT scanner with the slice thickness of 1.5 mm were imported into the open-source software for segmentation "3D Slicer".[29]

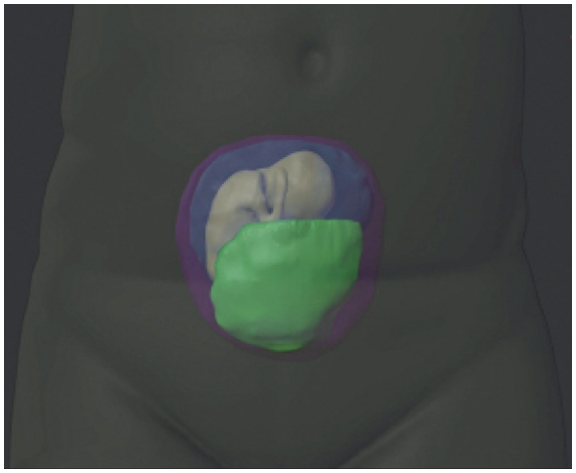

FIGURE 1. Magnified view of the computational phantom's lower abdomen and pelvis viewed as rendered polygon mesh in the computer 3D modeling software, showing the position of the 18-week-old fetus (in RST position) and placenta in relation to the uterus and the body of the mother. The fetus is shown in light gray colour, the amniotic fluid in transparent blue, the placenta in green, the uterus in transparent purple, and the body of the mother in olive green color.

Structure and organ segmentation and computer 3D modelling

In order to make the process of phantom development more understandable a schematic diagram was made and it is available in the manuscript supplement (Supplemental Figure 1). A combination of semi-automated and manual segmentation of the desired structures was performed in the aforementioned software for the generation of the polygon mesh of the organs. Later, three-dimensional (3D) CAD models of the same structures were exported as .STL files ("stereolithography", "standard tessellation language", a type of file used in CAD software and for 3D printing). Right paratracheal mediastinal lymphadenopathy and nodal mass in the right "rectus abdominis" muscle were omitted, as they were part of the patient's underlying disease, Hodgkin lymphoma.

Since the mother's head was not entirely captured by CT scanning, but up to the base of the skull, a CT scan of the whole head was taken from another patient with a similar physiognomy available in the open online DICOM data library (embodi3D, The biomedical 3D printing community, https://www.embodi3d.com/files/category/40-skull-head-and-neck-cts/). Then, polygon meshes and 3D models of the organs located in the head region were generated.

TABLE 1. List of the tissues and organs in our developed mesh pregnant female phantom in 2nd trimester (Tena), including volume, mass (calculated as the product of tissue density according to ICRP 89 and segmented organ volume) and surface area

Tissue/organ	Volume (cm^3)	Mass (g)	Surface area (cm^2)
Adrenal glands	5.1	5.2	40.2
Amniotic fluid	423.4	423.4	381.7
Blood vessels/blood	806.4	854.8	1739.3
Bones, cortex (including proximal humerus and femoral heads)	2443.4	4691.4	10667.3
Bone marrow (including proximal humerus and femoral heads)	723.4	724.4	2365.7
Central nervous system (brain and spinal cord)	1156.3	1214.1	752.4
Colon, content	454.2	472.4	825.5
Colon, wall	287.2	298.7	1914.3
Esophagus, content	4.4	0	42.0
Esophagus, wall	12.2	12.5	123.3
Eyeballs	12.4	13.1	32.9
Fetus, 17 week old	123.0	129.2	200.6
Gall bladder, content	15.5	15.9	42.3
Gall bladder, wall	15.6	16.1	104.1
Kidneys	312.3	327.9	340.4
Liver	1780.4	1869.5	1133.2
Lungs	3937.1	1515.8	2385.4
Myocardium	221.6	232.7	804.1
Pancreas	85.2	89.4	161.3
Parotid glands	24.1	24.9	64.8
Placenta	142.7	145.5	216.8
Soft tissues (muscles, adipose tissue and skin)	36080.4[1]	36802.0[2]	39186.9
Spleen	391.2	406.9	345.0
Stomach, duodenum and small intestine, content	570.3	593.1	1176.1
Stomach, duodenum and small intestine, wall	425.2	442.2	2717.9
Submandibular glands	5.3	5.5	22.0
Thyroid gland	10.0	10.4	3990.0
Upper airways (nasal cavity, pharynx and larynx) and trachea/air	136.9	0.1	426.7
Urinary bladder, content	11.1	11.6	38.6
Urinary bladder, wall	21.5	22.2	104.7
Uterus (myometrium)	552.5	580.1	917.6

[1] obtained by subtracting the sum of the volumes of all segmented organs and the total volume of the body;
[2] product of volume and 1.02 g/cm^3 which is the average value of muscle tissue density (1.050 g/cm^3), adipose tissue density (0.950 g/cm3) and skin density (1.060 g/cm^3)

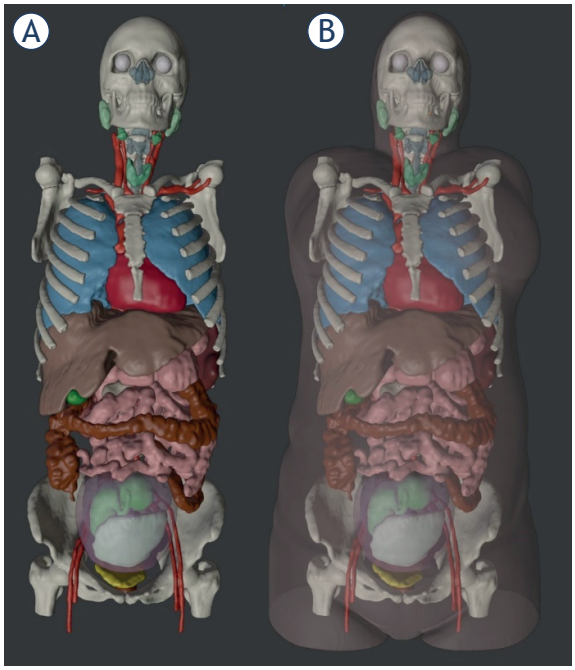

FIGURE 2. The mesh version of the Tena phantom without skin and soft tissues **(A)** and with the skin and soft tissues that are shown in transparent light brown color **(B)**. The uterus is shown in transparent purple for a better view of the fetus and its position in space and in relation to other organs.

The 17-week-old fetus, uterus, placenta, amniotic fluid, bladder, and small and large intestine were then segmented from the same patient's DICOM data obtained by MR scanning. The fetal head was positioned upwards, faced to the mother's left side of the body (right sacrum transverse (RST) position) as seen in Figure 1.

Certain bone structures such as the pelvis and both femoral heads were segmented from the MR examination as well, which then served as reference points for the registration of the organs in space (i.e. abdominal cavity). As the fetus, uterus, placenta and amniotic fluid were segmented from several different sequences of MR examination and the rest of the organs from the CT study, we could not perform a fusion of the several different studies and organ segmentation in the fused images using the "3D Slicer". Registration and correct positioning in space was performed manually by rotating and translating the objects using an open-source software Blender (Blender Foundation, Amsterdam, the Netherlands). The CAD models of the whole head including a skull, its associated organs and soft tissues were positioned according to the predefined bony structures of the pregnant female. The skull was merged with the rest of the skeleton and the upper airways were merged

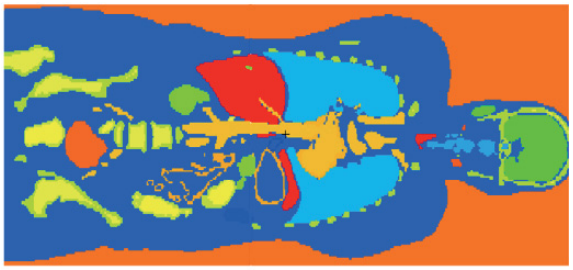

FIGURE 3. Voxelized phantom displayed using MCNP plotter.

with the pregnant female patient's trachea using the Blender CAD program and "Boolean Union" operation. The spatial resolution of the MR examination images has lower quality (thick slices and non-isovoxel) and the position of the bowels differs during pregnancy. For this reason, "Meshmixer" (Autodesk, Inc., California, U.S.A) CAM software was used for manual positioning and adjusting of the lower gastrointestinal tract (small and large intestine) according to the location of intestines obtained from MR examinations. The same actions were performed with the urinary bladder being slightly pushed towards the caudal.

After correct positioning of the bowels and the urinary bladder, using the "Meshmixer" and the "Offset" function, wall thickness was added to the esophagus, stomach, duodenum, small and large bowel, gall bladder and urinary bladder according to Proko.[30] In this way the lumen of the listed structures was created as follows: 2 mm for the esophagus, 6 mm for the stomach, 3 mm for the small bowel, 2 mm for the large bowel, 3 mm for the gall bladder and 4 mm for the urinary bladder.

Using the same CAM software, the head region was anonymized in such a manner that the facial features were altered beyond recognition (smoothing of the periorbital area, erasing of the mouth and ears).

Since our intention was to develop the phantom that is going to be suitable for various dosimetry studies, it was decided to remove both arms that were originally placed above the head during the CT scanning. The proximal part of both humerus as far as the surgical neck and both femurs down to the femoral neck were left in place since the proximal medulla of the humerus and femurs belongs to hematopoietic tissues in adults.

Development of the mesh phantom

Our phantom of a pregnant woman at the beginning of the second trimester has 31 structures, tissues and organs, seen in Figure 2 and listed in Table 1. This number is lower than in other similar phantoms (35 in RPI[23], 174 in UF[26] and 153 in Katja[24]) but we did not segment fetal structures separately due to the early stage of the fetus in our phantom. Also, we count all cortical bone and medullar bone as two structures and not separately by region as it is counted in other phantoms.

Conversion to imaging format

Exporting this dataset to DICOM presents more of a challenge. Firstly, a dataset is used as input to a multidimensional interpolation on a regular grid using scipy.[31] This allows the rescale structure set at an arbitrary resolution, so we use interpolation to derive a structure set on a sparser resolution typical for CT images in radiotherapy. Since the NRRD format contains only geometric information, without physical characteristics such as radiopacity, this information is determined from look-up tables and available curves relating to radiopacity and electron densities.[32] This allows for the reconstruction of a realistic CT image appropriate for input to a modern treatment planning system (TPS).

A separate problem is the definition of structure set in DICOM format since modern TPS typically do not support NRRD format. This is done through a workaround where another CT image set is defined, with geometry exactly like the previous but each structure is assigned with an unphysical, but distinct radiopacity. Such a spurious CT image set is imported into TPS just for the purpose to use ranger tools in order to locate each structure separately and save them to DICOM format. After the structure set is available in DICOM format, this spurious CT image set is discarded, and the structure set is used along with the realistically reconstructed CT image set for the purpose of treatment planning.

Conversion to the format for the computational dosimetry

The structure set has been exported from Slicer 3D[29] in NRRD format and imported into an in-house made software written in Python.[33] The structure set is defined as a set of overlapping bitwise masks defined on a dense cubic lattice, with approximately 1.8 mm per node. Such bitwise masks assign to each voxel a combination of covering structures and this dataset is appropriate for further processing. Exporting such a dataset to

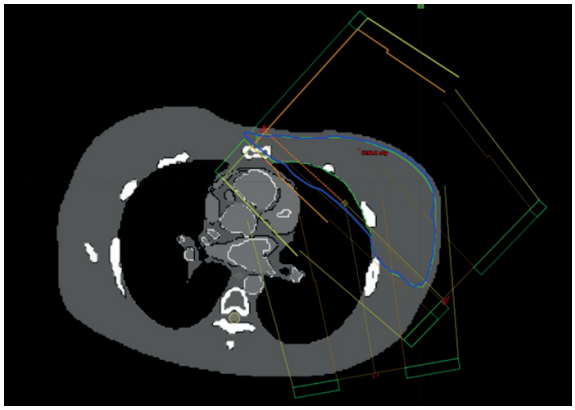

FIGURE 4. Beam arrangements in Eclipse.

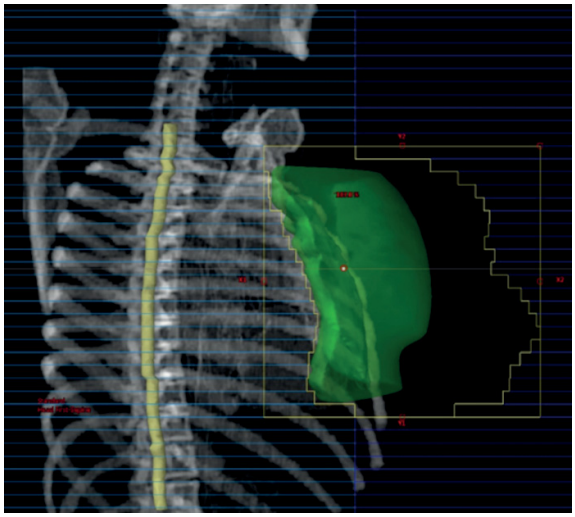

FIGURE 5. Beam Eye View of Field F1, where leafs are represented as transparent rectangles with blue edges. And PTV is colored in green.

the MCNP can be handled relatively easily, taking precautions regarding patient orientation and structure overlap which is not allowed since every voxel must have a uniquely defined chemical composition (Figure 3).

Generation of the physical phantom

As mentioned earlier in the text, phantom Tena could be obtained in its physical form for experimental dosimetry and is available for everyone to download. 3D modeling software "Blender" was used for the generation of the molds (available in Supplemental material as .STL files) for pouring the substitute tissue, thus generating a physical phantom as seen in the picture. Further description is beyond the scope of this article and will be explained in the upcoming research.

Radiotherapy plan

3D conformational radiotherapy treatment plan for the left breast irradiation was generated using Varian Eclipse 15.6 (Varian Medical Systems Inc., Palo Alto, USA) planning software. The plan was made for Siemens Oncor Expression machine using 6 MV beams. The plan consists of two main opposite fields in which beams are tangential to the chest wall. To guarantee a homogeneous dose in the breast (Planning Target Volume; PTV) three small (patch) fields are added to the main fields (Figure 4). The prescribed dose is 50 Gy in 25 fractions. The mean dose to the breast (PTV, 1688 cm^3) is 50.3 Gy and the maximum dose in the breast (PTV) is 53.5 Gy. The plan was achieved with five fields, denoted ad F1 to F5 in the text below (Figure 5). Minimal distance from the largest field (F1) used in radiotherapy plan is 22.5 cm, while the largest distance for the same field is 33 cm. For other fields these distances are even higher.

Monte Carlo simulations

Monte Carlo simulations were performed using Monte Carlo N-Particle transport code™ 6.2 (MCNP).[34] Siemens Oncor accelerator was modeled as it was described and extensively validated in our previous publications.[35-39] Parts included in the accelerator model are target, flattening filter, primary collimator, jaws, head shielding and monitor chamber. Each leaf in the multi leaf collimator is modeled independently and set up in the position that matches position in the accelerator head for corresponding field. Accelerator was modeled from electrons impinging the target with the energy of 6 MeV with a Gaussian spread of 3%. Each of the 80 leafs in the multi-leaf collimator was modeled separately and positioned to fit the field in the original radiotherapy plan. The phantom was placed in a separate universe, so the rotation of the phantom was achieved using the TR (transformation) card in the MCNP. In this way, it is relatively easy to achieve both rotation and translation of the phantom according to the accelerator head position at the same time. Phantom consisted of 219 x 148 x 479 voxels, and each of $1.55*10^7$ voxels have the dimensions of 0.186 x 0.186 x 0.186 cm^3 (Figure 3).

Materials for the phantom were used from ICRP 110 female phantom[40], and Compendium of Material Composition Data for Radiation Transport

TABLE 2. Tena phantom formats and their characteristics

Mesh format	DICOM	Voxelized
N° vertices[1]: 2889437 N° faces[1]: 5777800	Slice thickness: 0.625 mm Distance between slices: 1.867 mm Matrix: 512 x 512 Pixel dimensions: 0.82 mm	Grid size: 219 x 148 x 479 N° voxels: $1.55*10^{-7}$ Isovoxel size: 0.186 cm

[1] variable, could be decimated and adjusted to the computing power of the used computer

Modeling.[41] Since the breast is not segmented separately, TMESH tally was used to assess the breast dose for each applied field. Absorbed dose in the fetus was recorded using +F6 tally, while for obtaining the spectra in the fetus F4 tally was used. Each radiotherapy field is simulated independently with 10^{10} particles (electron impinging on target). DXTRAN sphere was set up around the fetus to speed up the calculations and to obtain each spectra bin with the minimum uncertainty possible. Spectra was collected in 200 energy bins ranging from 1 keV to 6 MeV. The results were accepted if the R-value fell below 0.1 and all 10 statistical checks were satisfied, meaning that out-of-field doses uncertainties in the fetal positions were below 10%.

MCNP provides results normalized per source particle (electron impinging on target) and both fetus and breast dose are normalized to the source particle. Each field contribution is taken from the TPS and multiplied with the dose calculated by MCNP. All 5 fields together have prescribed dose of 50 Gy (that is taken from TPS). In this way it is also possible to determine the field contribution to the fetus dose. To assess which field contributes the most to the fetal dose fetus/breast dose was calculated and expressed in mGy/Gy.

Results

Tena phantom

Within this study, three different formats of pregnant woman phantom in her 18th week of pregnancy were developed. All formats are available in the supplementary material of this paper. Characteristics of each format are given in Table 2.

Volumes of Tena organs compared with other available computational phantoms are shown in Supplemental Table 1. It can be seen, that the volumes of some structures differ, such as bones (cortex and bone marrow), upper airways, lungs, etc. This is possibly due to differences in the segmentation, counting of the structures in the phantoms, modeling of the other phantoms and phases of the CT scanning (during inspiration in our case). Structures like fetus, placenta, amniotic fluid and uterus (myometrium) also differ, but that is due to the different fetal gestational ages of the compared phantoms.

Characterization of fetus dose during photon breast radiotherapy

A radiotherapy plan with 5 RT fields gave beam contributions as shown in Table 3. Results of the

TABLE 3. Contribution of each field to the fetal dose. Fetus and breast doses are normalized per source particle, field contribution to the breast dose is obtained from treatment planning system (TPS), and the breast/fetus ratio is calculated from normalized breast and fetus doses

Field	Fetus dose per source particle [Gy/SP] 10^{-19}	Breast dose per source particle [Gy/SP] 10^{-19}	Field contribution to breast dose[1]	Fetus dose normalized to field contribution [Gy/SP] 10^{-19}	Breast dose normalized to field contribution [Gy/SP] 10^{-19}	Ratio fetus / breast dose [mGy/Gy]
F1	1.45 ± 0.12	1000 ± 90	0.437	0.634 ± 0.054	437 ± 37	1.44
F2	1.05 ± 0.09	1070 ± 90	0.378	0.399 ± 0,035	404 ± 36	0.99
F3	1.03 ± 0.08	993 ± 80	0.064	0.066 ± 0,005	63.5 ± 5	1.03
F4	0.270 ± 0.02	1010 ± 80	0.057	0.015 ± 0.001	57.3 ± 4	0.27
F5	0.854 ± 0.07	449 ± 40	0.064	0.055 ± 0,005	28.7 ± 2	1.91
Total				1.169 ± 0.064	992.5 ± 52	
Total normalized to prescribed dose				58.9 ± 3.7 mGy	50 Gy*	

[1] obtained from TPS

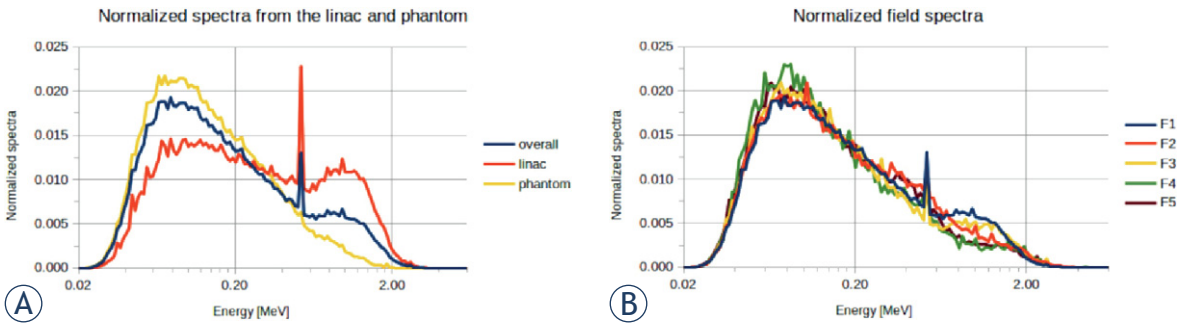

FIGURE 6. Spectra for F1 of the photons coming from the accelerator head and all the photons reaching the fetus **(A)**; Photon spectra in fetus for each field **(B)**.

fetus and breast dose, normalized per source particle were determined using MC simulations (Table 3).

Since the prescribed dose to the breast was 50 Gy, according to the data shown in Table 3 it is easy to calculate that the whole fetus will receive 58.9 mGy (with uncerintaity of 3.7 mGy).

As it can be seen from Figure 4 and Table 3, field F1 is a medial field with the major contribution to the breast dose while F2 is a lateral field. The other three patch fields with significantly lower breast dose contribution are F3 (medial), F4 (lateral) and F5 (posterior). From the fetus/breast dose ratio it is obvious that medial fields have a higher contribution to the fetal dose, while the most dominant contribution comes from the posterior F5 field.

Monte Carlo simulations enabled us to determine the place of the origin of all the photons reaching the fetus during breast radiotherapy. These data are shown in Table 4 and display the amount of the photons that are reaching the fetus and are caused by the accelerator's head leakage, or they are created within the mother. It is interesting to see that 90.5% of all the photons in the fetus are created within the mother, while only 9.5% of them are created in the accelerator's head.

Our final intention is to develop a physical phantom and perform experimental measurements using this phantom. We also evaluated the energy spectra reaching the fetus as some of the passive dosimeters can be energy-dependent. Figure 6 shows these spectra and separately display photons coming from the linac head and the mother body. It can be seen that photons that reach the fetus and are coming from the linac head have higher energies (average energy 0.43 MeV) while photons that are coming from the mother mainly originate from secondary interactions and have an average energy of 0.2 MeV.

TABLE 4. Relative contribution to the absorbed dose in the fetus (%) originating in the linac or the phantom. The ratio for each field of photons originating in linac or phantom is given in the last row

	F1	F2	F3	F4	F5	Overall
Linac (%)	6.0	2.1	0.8	0.3	0.3	9.5
Phantom (%)	37.7	35.7	5.6	5.4	6.1	90.5
Contribution ratio	16.12	5.8	14.3	5.5	4.9	

Discussion

Within this paper computational phantom of 37-year old woman in her 18th week of pregnancy was created based on CT and MRI images of the pregnant patient. To the best of our knowledge, this is the first pregnant phantom made directly from the MRI images of the pregnant patient and not done by inserting the fetus into the non-pregnant patient. To make the implementation of the phantom in the TPS possible, the DICOM format was prepared. Voxelized format, that is suitable for MC simulations, and STL format, suitable for 3D printing of molds, is also provided as a supplement to this paper. In this way, we are making possible usage of the same phantom in TPS, MC simulations and experiments once the physical representation of the phantom is going to be available.

As a proof of feasibility, a typical breast cancer plan was prepared in order to assess the dose received by the fetus during the breast cancer radiotherapy as well as to characterize the field (determine its spectra) reaching the detector. This information is important to set up experiments in the future as detectors, such as thermoluminescent detectors (TLDs), are characterized by a varying response as a function of photon energy,

which has been characterized experimentally and through modeling.[42] Input from simulations will be important for an optimal selection of detector type(s) and/or correction of this energy response may be required.

In clinical practice TPS is not able to estimate the dose to the fetus since its cutoff line for dose calculations is mostly positioned above the uterus. However, our results indicate that the fetus is going to receive only a small fraction of the dose delivered to the breast. As was mentioned earlier fetus receives the dose of 59 mGy (with the simulations uncertainty of 8%), which is close to the threshold of 50 mGy prescribed by the ICRP[15] and well below 100 mGy. It is also worth mentioning that no shielding to the fetus was applied. In the study published by Bednarz *et al*. dose of 120 mGy to the fetus was determined when the mantle was irradiated with 39 Gy with only one gantry field.[43] This is two times higher when compared to our results although no leafs are simulated in the mentioned study. Antypas *et al*. experimentally determined the dose of 39 mGy to the fetus, when 49 Gy to the breast, using two fields, was applied, which is in line with our results.[18] Several experimental studies have also determined the dose to the fetus, namely van der Giessen *et al*. reported 280 mGy to the fetus when 50 Gy to the breast was applied[20] and Ngu *et al*. reported 210 mGy with similar conditions only without shielding.[19] Mazonakis *et al*. computationally determined the dose of 131 mGy when 50 Gy to the breast of the pregnant phantom was applied without shielding.[44] These doses are all significantly higher than the dose that we determined. The cause for the large range of published fetal doses during breast radiotherapy could come due to different phantom anatomy, fetal position or gestation period, breast size and position as well as different optimization of the radiotherapy treatment plans. We will further investigate this in the future.

Our study has limitations such as Monte Carlo simulations are normalized per source particle (electron impinging on accelerator target). Besides validation experiment is not performed yet since it is planned in our future work to make a physical representation of the phantom. The phantom is made according to the anatomical data found. Nevertheless, the fetal dose during photon breast radiotherapy will differ if the patient change or if fetal position within the patient change.

Knowing each field contribution to the fetal dose, that dose can be further optimized. From the relative dose contribution to the fetus, it can be easily concluded that F5 has the largest fetus/breast ratio, followed by field F1. This result is important since the new radiotherapy plan can be tailored according to the information obtained by MC and additional reduction to the dose can be achieved by avoiding fields F5 and F1 and giving more significance to the lateral fields.

In our simulated case 9.5% of the absorbed dose in the fetus is caused by the accelerator head leakage, while 90.5% of the absorbed dose comes through the patient's body. In the literature, those values differ significantly i.e. van der Giessen in the case report states that 35% of the fetal dose comes as scattered radiation using 10 MeV X-ray beams.[20] According to Stovall *et al*., collimator scatter is the dominant component of the fetal dose at larger distances (70–90 cm) from the primary radiation field.[45] Chofor *et al*. and Mazonakis *et al*. also state that the head leakage and head scatter radiation are dominant components in fetal dose at the larger distances from the primary beam edge.[46,47] Our data correlate to Ngu *et al*. report who states that most of the secondary photons come as scattered radiation, while a smaller portion comes as leakage radiation from the linear accelerator head.[19] The data on accelerator head leakage, that reaches the fetus, depend on the accelerator type and the shielding application.[48] As already mentioned shielding is one important topic when RT is applied to pregnant women. Lead is the most commonly used apron for covering the patient during radiotherapy has an HVL (half-value layer) of 7.9 mm at the energy of 1 MeV that is comparable to our results (Figure 6B). It means that an apron of 30 x 30 cm^2 dimensions would have approximately 80 kg, and it is probably inappropriate to be positioned on the pregnant woman's belly, but rather lead shield on the rigged frame could be used as proposed by some authors.[13,19,45]

In the near future, our intention is to produce a low -cost physical phantom using a three-dimensional (3D) printer for mold making and pouring substitute tissues into 3D printed molds. Our estimation is that all the components for molding and casting such phantom is in order of 1000 €. It is our intention to validate our model experimentally and complete both experimental and computational results. Once a completed physical representation of the phantom can be further used in other fields such as interventional and diagnostic radiology and determination of dose for both patients and staff. Proton therapy of pregnant patients is also a topic of interest[49], our newly developed phantom can provide new insights into this field too.

Conclusions

Developed phantom offers the possibility to perform treatment planning and Monte Carlo on the same pregnant female phantom. There is also a possibility for 3D printing the same phantom which would enable experimental measurements on the identical geometry. This is important for the improvement of current dosimetry practices in clinics enabling more consensus on such treatments and ultimately for the optimization of such treatments. Our feasibility study demonstrated that the dose received by the fetus, during photon breast radiotherapy was just above the recommended level (59 mGy for the 50 Gy prescribed to the breast) which demonstrates the need to have good dosimetry tools in place for dose assessment and optimization. Within this study, the spectra of photon reaching the fetus are also determined, which will simplify the selection of appropriate detectors once when the physical representation of the phantom is going to be available.

Acknowledgments

This research is made as a part of the EURADOS WG9 and WG6 activities. It is financed by the Institutional projects IP3-2022 of the Faculty of Medicine in Osijek and IP4-2021 in the Faculty of Dental Medicine and Health in Osijek.

Special thanks to the pregnant woman T. Š. who allowed us to use her diagnostic images for research purposes and the development of this phantom.

References

1. Basta P, Bak A, Roszkowski K. Cancer treatment in pregnant women. *Contemp Oncol* 2015; **19:** 354-60. doi: 10.5114/wo.2014.46236
2. Botha MH, Rajaram S, Karunaratne K. Cancer in pregnancy. *Int J Gynecol Obstet* 2018; **143:** 137-42. doi: 10.1002/ijgo.12621
3. Kal HB, Struikmans H. Radiotherapy during pregnancy: fact and fiction. *Lancet Oncol* 2005; **6:** 328-33. doi: 10.1016/S1470-2045(05)70169-8
4. Fenig E, Mishaeli M, Kalish Y, Lishner M. Pregnancy and radiation. *Cancer Treat Rev* 2001; **27:** 1-7. doi: 10.1053/ctrv.2000.0193
5. Leonardi M, Cecconi A, Luraschi R, Rondi E, Cattani F, Lazzari R, et al. Electron beam intraoperative radiotherapy (ELIOT) in pregnant women with breast cancer: from in vivo dosimetry to clinical practice. *Breast Care* 2017; **12:** 396-400. doi: 10.1159/000479862
6. Shlensky V, Hallmeyer S, Juarez L, Parilla B V. Management of breast cancer during pregnancy: are we compliant with current guidelines? *Am J Perinatol Reports* 2017; **7:** e39-43. doi: 10.1055/s-0037-1599133
7. De Santis M, Di Gianantonio E, Straface G, Cavaliere AF, Caruso A, Schiavon F, et al. Ionizing radiations in pregnancy and teratogenesis: a review of literature. *Reprod Toxicol* 2005; **20:** 323-9. doi: 10.1016/j.reprotox.2005.04.004
8. Burdorf A, Figà-Talamanca I, Jensen TK, Thulstrup AM. Effects of occupational exposure on the reproductive system: core evidence and practical implications. *Occup Med* 2006; **56:** 516-20. doi: 10.1093/occmed/kql113
9. International Commission on Radiological Protection. Protection IC on R. ICRP publication 84 – pregnancy and medical radiation. *Ann ICRP*. 2000; **30(1):** 43.
10. Smith H, International Commission on Radiological Protection. *1990 recommendations of the International Commission on Radiological Protection*. ICRP Publication 60. Oxford: Pergamon press; 1991. [cited 2022 Jun 15]. Available at: https://www.icrp.org/publication.asp?id=icrp%20publication%2060
11. Organization for Occupational Radiation Safety in Interventional Fluoroscopy. *Occupational exposure to ionizing radiation in interventional fluoroscopy: severity of adverse effects of a growing health problem*. Washington D.C.: ORSIF; 2015.
12. Amant F, Han SN, Gziri MM, Vandenbroucke T, Verheecke M, Van Calsteren K. Management of cancer in pregnancy. *Best Pract Res Clin Obstet Gynaecol* 2015; **29:** 741-53. doi: 10.1016/j.bpobgyn.2015.02.006
13. Wallack MK, Wolf Jr JA, Bedwinek J, Denes AE, Glasgow G, Kumar B, et al. Gestational carcinoma of the female breast. *Curr Probl Cancer* 1983; **7:** 1-58. doi: 10.1016/s0147-0272(83)80006-3
14. Royal College of Obstetricians and Gynaecologists. Pregnancy and breast cancer. *RCOG Green-top Guidel No 12;* 2011.
15. Streffer C, Shore R, Konermann G, Meadows A, Holm LE, Stather J, et al. Biological effects after prenatal irradiation (embryo and fetus). A report of the International Commission on Radiological Protection. *Ann ICRP* 2003; **33(1-2):** 5-206. PMID: 12963090
16. Gorson RO, Brent RL, Moseley RD. Medical radiation exposure of pregnant and potentially pregnant women. *Natl Counc Radiat Prot Meas Rep* 1977; **54:** 70-100.
17. Brent RL, Frush DP, Harms RW, Linet MS. Preconception and prenatal radiation exposure: health effects and protective guidance. NCRP No. 174. *Sel Work Robert Brent* 2013; **39**.
18. Antypas C, Sandilos P, Kouvaris J, Balafouta E, Karinou E, Kollaros N, et al. Fetal dose evaluation during breast cancer radiotherapy. *Int J Radiat Oncol Biol Phys* 1998; **40:** 995-9. doi: 10.1016/s0360-3016(97)00909-7
19. Ngu SLC, DuvalL P, Collins C. Foetal radiation dose in radiotherapy for breast cancer. *Australas Radiol* 1992; **36:** 321-2. doi: 10.1111/j.1440-1673.1992.tb03209.x
20. Van der Giessen P-H. Measurement of the peripheral dose for the tangential breast treatment technique with Co-60 gamma radiation and high energy X-rays. *Radiother Oncol* 1997; **42:** 257-64. doi: 10.1016/s0167-8140(96)01884-1
21. *Handbook of anatomical models for radiation dosimetry*. Xu XG, Eckerman KF, editors. Boca Raton: CRC Press; 2009. doi: 10.1201/EBK1420059793
22. Anderson CA, Kelley KC, Goorley JT. *Mesh human phantoms with MCNP*. Los Alamos, NM (United States): Los Alamos National Lab.(LANL); 2012.
23. Xu XG, Taranenko V, Zhang J, Shi C. A boundary-representation method for designing whole-body radiation dosimetry models: pregnant females at the ends of three gestational periods – RPI-P3,-P6 and-P9. *Phys Med Biol* 2007; **52:** 7023-44. doi: 10.1088/0031-9155/52/23/017
24. Becker J, Zankl M, Fill U, Hoeschen C. Katja – the 24th week of virtual pregnancy for dosimetric calculations. *Polish J Med Phys Eng* 2008; **14:** 13-20. doi: 10.2478/v10013-008-0002-4
25. Maynard MR, Long NS, Moawad NS, Shifrin RY, Geyer AM, Fong G, et al. The UF Family of hybrid phantoms of the pregnant female for computational radiation dosimetry. *Phys Med Biol* 2014; **59:** 4325-43. doi: 10.1088/0031-9155/59/15/4325
26. Paulbeck C, Griffin K, Lee C, Cullings H, Egbert SD, Funamoto S, et al. Dosimetric impact of a new computational voxel phantom series for the Japanese atomic bomb survivors: pregnant females. *Radiat Res* 2019; **192:** 538-61. doi: 10.1667/RR15394.1
27. Xu XG. An exponential growth of computational phantom research in radiation protection, imaging, and radiotherapy: a review of the fifty-year history. *Phys Med Biol* 2014; **59:** R233-302. doi: 10.1088/0031-9155/59/18/R233

28. International Commission on Radiological Protection. Basic anatomical and physiological data for use in radiological protection: reference values. ICRP Publication 89. *Ann ICRP* 2002; **32(3-4):** 1-277.

29. Kikinis R, Pieper SD, Vosburgh KG. 3D Slicer: a platform for subject-specific image analysis, visualization, and clinical support. In: *Intraoperative imaging and image-guided therapy*. Springer; 2014. p. 277-89. doi: 10.1007/978-1-4614-7657-3_19

30. Prokop M. *Spiral and multislice computed tomography of the body*. Thieme Medical Publishers; 2003.

31. Virtanen P, Gommers R, Oliphant TE, Haberland M, Reddy T, Cournapeau D, et al. SciPy 1.0: fundamental algorithms for scientific computing in Python. *Nat Methods* 2020; **17:** 261-72. doi: 10.1038/s41592-019-0686-2

32. White DR, Griffith RV, Wilson IN. ICRU Report 46. Photon, electron, proton and neutron interaction data for body tissues. *J Int Comm Radiat Units Meas* 1992; **1:** NP.

33. Van Rossum G, Drake FL. *Python reference manual.* iUniverse Indiana; 2000.

34. Werner CJ, Bull JS, Solomon CJ, Brown FB, McKinney GW, Rising ME, et al. *MCNP version 6.2 Release notes*. Report LA-UR-18-20808. Los Alamos Natl Lab; 2018.

35. Brkić H, Ivković A, Kasabašić M, Poje Sovilj M, Jurković S, Štimac D, et al. The influence of field size and off-axis distance on photoneutron spectra of the 18 MV Siemens Oncor linear accelerator beam. *Radiat Meas* 2016; **93:** 28-34. doi: 10.1016/j.radmeas.2016.07.002

36. Ivković A, Faj D, Galić S, Karimi AH, Kasabašić M, Brkić H. Accuracy of empirical formulas in evaluation of neutron dose equivalent inside the ^{60}Co vaults reconstructed for medical linear accelerators. *Int J Radiat Res* 2020;**18:** 99-107. doi: 10.18869/acadpub.ijrr.18.1.99

37. Kolacio MŠ, Brkić H, Faj D, Radojčić ĐS, Rajlić D, Obajdin N, et al. Validation of two calculation options built in Elekta Monaco Monte Carlo based algorithm using MCNP code. *Radiat Phys Chem* 2021; **179:** 109237. doi: 10.1016/j.radphyschem.2020.109237

38. Vukovic B, Faj D, Poje M, Varga M, Radolic V, Miklavcic I, et al. A neutron track etch detector for electron linear accelerators in radiotherapy. *Radiol Oncol* 2010; **44:** 62-6. 10.2478/v10019-010-0003-2

39. Brkić H, Kasabašić M, Ivković A, Agić D, Krpan I, Faj D. Influence of head cover on the neutron dose equivalent in Monte Carlo simulations of high energy medical linear accelerator. *Nucl Technol Radiat Prot* 2018; **33:** 217-22. doi: 10.2298/NTRP1802217B

40. Zankl M. Adult male and female reference computational phantoms (ICRP Publication 110). *Japanese J Heal Phys* 2010; **45:** 357-69. 10.5453/JHPS.45.357

41. Detwiler R, McConn R, Grimes T, Upton S, Engel E. Compendium of material composition data for radiation transport modeling [Internet]. Richland, WA (United States): Pacific Northwest National Lab. (PNNL); [cited 2022 May 15]. doi: 10.2172/1782721. Available from: https://www.osti.gov/servlets/purl/1782721/

42. Parisi A, Dabin J, Schoonjans W, Van Hoey O, Mégret P, Vanhavere F. Photon energy response of LiF: Mg, Ti (MTS) and LiF: Mg, Cu, P (MCP) thermoluminescent detectors: experimental measurements and microdosimetric modeling. *Radiat Phys Chem* 2019; **163:** 67-73. doi: 10.1016/j.radphyschem.2019.05.021

43. Bednarz B, Xu XG. A feasibility study to calculate unshielded fetal doses to pregnant patients in 6-MV photon treatments using Monte Carlo methods and anatomically realistic phantoms. *Med Phys* 2008; **35:** 3054-61. doi: 10.1118/1.2938519

44. Mazonakis M, Tzedakis A, Damilakis J. Monte Carlo simulation of radiotherapy for breast cancer in pregnant patients: how to reduce the radiation dose and risks to fetus? *Radiat Prot Dosimetry* 2017; **175:** 10-6. doi: 10.1093/rpd/ncw260

45. Stovall M, Blackwell CR, Cundiff J, Novack DH, Palta JR, Wagner LK, et al. Fetal dose from radiotherapy with photon beams: report of AAPM Radiation Therapy Committee Task Group No. 36. *Med Phys* 1995; **22:** 63-82. doi: 10.1118/1.597525

46. Chofor N, Harder D, Willborn KC, Poppe B. Internal scatter, the unavoidable major component of the peripheral dose in photon-beam radiotherapy. *Phys Med Biol* 2012; **57:** 1733-43. doi: 10.1088/0031-9155/57/6/1733

47. Mazonakis M, Damilakis J. Estimation and reduction of the radiation dose to the fetus from external-beam radiotherapy. *Phys Medica* 2017; **43:** 148-52. doi: 10.1016/j.ejmp.2017.09.130

48. Schneider T, Stoll E. Molecular-dynamics study of a three-dimensional one-component model for distortive phase transitions. *Phys Rev B* 1978; **17:** 1302. doi: 10.1103/PhysRevB.17.1302

49. De Saint-Hubert M, Tymińska K, Stolarczyk L, Brkić H. Fetus dose calculation during proton therapy of pregnant phantoms using MCNPX and MCNP6. 2 codes. *Radiat Meas* 2021; **149:** 1-7. 106665. doi: 10.1016/j.radmeas.2021.106665